Journal of Colloid and Interface Science 655 (2024) 286–295

Contents lists available at ScienceDirect

Journal of Colloid And Interface Science

journal homepage: www.elsevier.com/locate/jcis

Magnetic-driven Interleukin-4 internalization promotes magnetic nanoparticle morphology and size-dependent macrophage polarization

Ángela Arnosa-Prieto [a,*], Patricia Diaz-Rodriguez [b,*], Manuel A. González-Gómez [a], Pelayo García-Acevedo [a], Lisandra de Castro-Alves [a], Yolanda Piñeiro [a], José Rivas [a]

[a] NANOMAG Laboratory, Applied Physics Department, Materials Institute (iMATUS) and Health Research Institute of Santiago de Compostela (IDIS), Universidade de Santiago de Compostela, Santiago de Compostela 15706, Spain
[b] Departamento de Farmacología, Farmacia y Tecnología Farmacéutica, Grupo I+D Farma (GI-1645), Instituto de Materiales (iMATUS), Instituto de Investigación Sanitaria de Santiago de Compostela (IDIS), Universidade de Santiago de Compostela, Santiago de Compostela 15782, Spain

GRAPHICAL ABSTRACT

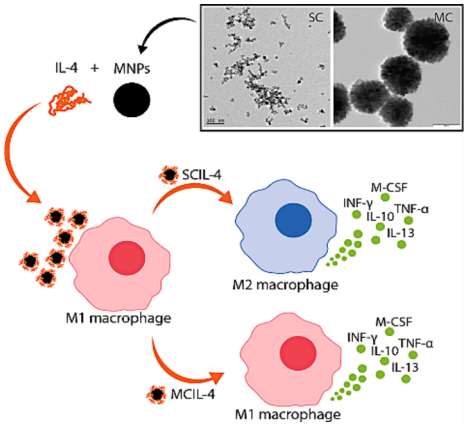

ARTICLE INFO

Keywords:
Magnetic nanoparticle
Iron oxide
Interleukin-4
Macrophage polarization
M1
M2

ABSTRACT

Macrophages are known to depict two major phenotypes: classically activated macrophages (M1), associated with high production of pro-inflammatory cytokines, and alternatively activated macrophages (M2), which present an anti-inflammatory function. A precise control over M1-M2 polarization is a promising strategy in therapeutics to modulate both tissue regeneration and tumor progression processes. However, this is not a simple task as macrophages behave differently depending on the microenvironment. In agreement with this, non-consistent data have been reported regarding macrophages response to magnetic iron oxide nanoparticles (MNPs). To investigate the impact of both tissue microenvironment and MNPs properties on the obtained macrophage responses, single-core (SC) and multi-core (MC) citrate coated MNPs, are synthesized and, afterwards, loaded with a macrophage polarization trigger, IL-4. The developed MNPs are then tested in macrophages subjected to different stimuli. We demonstrate that macrophages treated with low concentrations of MNPs behave differently depending on the polarization stage independently of the concentration of iron. Moreover, we

* Corresponding authors.
E-mail addresses: angela.arnosa@usc.es (Á. Arnosa-Prieto), patricia.diaz.rodriguez@usc.es (P. Diaz-Rodriguez).

https://doi.org/10.1016/j.jcis.2023.11.004
Received 26 May 2023; Received in revised form 27 October 2023; Accepted 1 November 2023
Available online 4 November 2023

find out that MNPs size and morphology determines the effect of the IL-4 loaded MNPs on M1 macrophages, since IL-4 loaded SC MNPs favor the polarization of M1 macrophages towards M2 phenotype, while IL-4 loaded MC MNPs further stimulate the secretion of pro-inflammatory cytokines.

1. Introduction

Macrophages are immune cells with a critical role in the immune response against pathogenic infections, as well as an involvement in tissue homeostasis, tissue repair and development. The different contributions of macrophages in these processes depend in their polarization stage. Macrophage polarization entails the exhibition of specific phenotype and a functional response to the environmental stimuli and signals [1]. Macrophages present two major phenotypes with different functions: the classically activated macrophages, hereafter M1, and the alternatively activated macrophages, hereafter M2. M1 phenotype is characterized by being associated with high production of pro-inflammatory cytokines, leading to an inflammatory response to clear pathogens and the damaged tissue at the initial state of a wound healing process. M2 macrophages, known as wound-healing macrophages, promote the healing and regeneration process and are also associated to tumor progression and metastasis. These cells present an anti-inflammatory function, as well as pro-regenerative role [2,3].

Cytokines are one of the several stimulatory factors that lead macrophages to polarization towards M1 or M2. INF-γ, TNF-α or M-CSF are pro-inflammatory cytokines that can provoke M1 polarization, while IL-10, IL-6 or IL-4 are anti-inflammatory cytokines that stimulate M2 polarization [4,5].

Although many cell types are involved in tissue recovery processes, because of their high plasticity, macrophages have been shown to present critical regulatory activity at all stages of repair and regeneration [6,7]. As an example, in bone regeneration, osteal macrophages play a key role in the regulation of bone healing, for being able to instruct bone regeneration upon biomaterials implantation [8,9]. In repair and regeneration processes, after the recession of the early inflammatory phase, the predominant macrophage population adopts a wound-healing phenotype, identified by the production of numerous growth factors. An amplified or prologued pro-inflammatory phase and a deficiency of anti-inflammation can lead to unsuccessful regeneration causing bone fractures [10,11]. The transition from the inflammatory (M1) to the anti-inflammatory (M2) phase is a key step in regulating the presence of different macrophage subtypes and the promotion of tissue regeneration [12].

On the other hand, the re-education of macrophages by inducing an M2 to M1 switch, can be used to regulate tumor development [13,14]. Tumor-associated macrophages (TAMs) are macrophages found in the tumor microenvironment (TME). These macrophages have been reported to show at higher extend a M2 polarization profile compared to M1. TAMs are highly dependent on the stimuli present within the TME, where the population of M2 macrophages acts enhancing the tumor cell growth [15]. The possibility to re-educate TAM by repolarizing the protumoral M2 macrophages towards tumoricidal M1 macrophages directs the attention to its use as a therapeutic approach in restraining tumor progression [16–19].

Therefore, a precise control on M1-M2 polarization during tissue repair and tumor progression processes can be a promising strategy in therapeutics [20–22]. Different methods can be used to reprogram macrophages for therapeutic purposes. Some of the most common methods are targeted antibody treatments [23], small molecule drugs [24,25] and gene expression modification using viral vectors [26,27], naked nucleic acids [28] and artificial nucleic acids carriers or nanovectors [29]. In addition to nucleic acid delivery, nanoparticles can be loaded with therapeutic molecules for macrophage targeting and polarization control [30,31].

Among all the nanoparticles, iron oxide magnetic nanoparticles (MNPs) have shown promising results as nanocarriers for therapy and as contrast agents for magnetic resonance imaging [32–34]. They present a wide variety of possibilities for surface modification, easily scaling-up synthesis and advantageous magnetic properties [35]. The impacts of iron oxide nanoparticles used as contrast agents in macrophages [36] have been previously reported. Likewise, their effects as inhibitors of tumor growth through macrophage polarization [37] and as reductors of macrophage inflammatory response in tissue regeneration [38] have been previously tested with inconsistent results depending on the nanoparticles sizes, concentrations and the specific study.

To elucidate the role of macrophage microenvironment and the nanoparticles properties on the obtained macrophage response, single-core (SC) and multi-core (MC) citrate coated iron oxide magnetic nanoparticles were prepared and tethered with a macrophage polarization trigger, IL-4. Plain MNPs and IL-4 loaded MNPs were then tested on naïve and M1 human macrophages. Moreover, loaded MNPs were internalized in M1 macrophages through passive transfection and magnetotransfection. The effect of the size, concentration and transfection modality was studied through the analysis of the macrophages secrotome profile. Passive transfection studies showed that IL-4 loaded SC (SCIL-4) produced a decrease in the pro-inflammatory cytokines secretion of M1 macrophages compared to non-treated cells, while IL-4 loaded MC (MCIL-4) produced the opposite effect by increasing the pro-inflammatory cytokines secretion. In the case of magnetotransfection, SCIL-4 NPs did not produce a significant effect while MCIL-4 NPs promoted an increased secretion of pro-inflammatory cytokines. However, when increasing the MNPs concentration, SCIL-4 NPs achieved an anti-inflammatory cytokines secretion profile, while MCIL-4 NPs raised the production pro-inflammatory M-CSF and TNF-α. These results help to understand the macrophages responses to MNPs pointing out, for the first time, that these cells respond differently to the nanoparticles depending on the polarization stage. This finding would be useful to tailor the macrophages responses in both regeneration processes and tumor progression control.

2. Materials and methods

2.1. Materials

Iron trichlorhide hexahydrate ($FeCl_3{\cdot}6H_2O$, 99 %), iron sulfate heptahydrate ($FeSO_4{\cdot}7H_2O$, 99 %), ammonium hydroxide solution (NH_4OH, 28 %), sodium citrate dihydrate ($C_6H_9Na_3O_9{\cdot}2H_2O$, 98 %), sodium acetate anhydrous ($C_2H_3NaO_2$, 99 %), N-(3-Dimethylaminopropyl)-N′-ethylcarbodiimide hydrochloride (EDC, 98 %), N-hydroxysulfosuccinimide sodium salt (sulfo-NHS, 98 %), bovine serum albumin (BSA, 98 %) and phorbol 12-myristate 13-acetate were obtained from Sigma-Aldrich (Germany). Ethanol (C_2H_6O, absolute) was purchased from Merck (Germany). Ethylene glycol ($C_2H_6O_2$, 95 %) was obtained from Fluka (Switzerland). Hydrochloric acid (HCl, 37 %) was obtained from Acros Organics (Belgium). Cyclohexane (C_6H_{12}, 99 %) was purchased from Alfa Aesar (UK). Recombinant human interleukin 4 (IL-4) was purchased from Gibco (USA). Monocytes cell line, THP-1 (TIB-202), were obtained from ATCC (USA). Fetal bovine serum (FBS), Roswell Park Memorial Institute 1640 Medium (RPMI 1640), antibiotic solution (10.000 units/mL penicillin, 10.000 μg/mL streptomycin) cell culture grade 2-mercaptoethanol and Dulbecco's Modified phosphate buffered saline (DPBS) were obtained from Gibco (USA). Cell Proliferation Reagent WST-1 was purchased from Roche (Switzerland). Milli-Q (Millipore®, Burlington, MA, USA) deionized water, and cell culture grade water purchased from Corning were used in all the experiments. Cell

culture grade water was used in all the experiments unless the use of Milli-Q water is indicated. All chemicals were used without any further purification.

2.2. Synthesis of single-core citrate coated iron oxide nanoparticles (SC)

$FeCl_3{\cdot}6H_2O$ (45 mmol) and $FeSO_4{\cdot}7H_2O$ (30 mmol) were dissolved in HCl (100 mL, 10 mM) with mechanical stirring at 220 rpm for 30 min at room temperature. Next, the temperature was raised to 60 °C and NH_4OH (30 mL) was added to the solution, and it was allowed to react for 1 h. After that time, sodium citrate (170 mmol) was added, and the mixture was heated up to 95 °C and the temperature was maintained for 2 h. After that time, the pH was adjusted to 4 with HCl (9 %). The obtained nanoparticles were magnetically isolated, washed four times with Milli-Q water and suspended in cell culture grade water. Thermogravimetric analysis revealed a composition of 63.6 % of Fe_3O_4 per NP.

2.3. Synthesis of multi-core citrate coated iron oxide nanoparticles (MC)

Multi-core citrate coated iron oxide nanoparticles were obtained by a solvothermal process described by Jiang [39]. $FeCl_3{\cdot}6H_2O$ (3.8 mmol), sodium citrate (0.41 mmol) and sodium acetate (33 mmol) were dissolved in ethylene glycol (30 mL) with mechanical stirring at 150 rpm until the solution process was completed. The solution was transferred to a 50 mL Teflon-lined stainless-steel autoclave. The autoclave was heated to 200 °C for 15 h, and then cooled to room temperature naturally. The product was magnetically isolated with a NdFeB magnet and washed three times with ethanol and five times with Milli-Q water. Finally, the MNPs were redispersed in cell culture grade water. Thermogravimetric analysis revealed a composition of 68.2 % of Fe_3O_4 per NP.

2.4. Adsorption of BSA on MNPs

To evaluate the adsorption of BSA on the nanoparticles surface, several tests were carried out at different incubation times. For that, nanoparticles (1 mg mL^{-1} in PBS) were mixed with BSA (50 μg mL^{-1} in PBS) in a total volume of 400 μL. The suspensions were incubated for 2 and 4 h at room temperature and 24 h at 4 °C. Then, the MNPs were centrifuged at 13300 rpm for 15 min at 4 °C and the supernatant was used to analyze the adsorption efficiency with a Micro BCA™ Protein Assay Kit.

2.5. Functionalization of MNPs with BSA

The procedure for the functionalization of MNPs with BSA is based on a previously published protocol [40] and was carried out as it follows. EDC (100 μL, 43 mM) and sulfo-NHS (100 μL, 65 mM) were added to a MNPs' suspension (800 μL, 1.25 mg mL^{-1}) in MES (50 mM). The mixture was incubated for 30 min at 37 °C with orbital shaking at 200 rpm. Then, the MNPs were washed twice with water and resuspended in H_2O (990 μL). Later, BSA (10 μL, 5 mg mL^{-1}) was added to the MNPs and the mixture was incubated overnight at 37 °C with orbital shaking at 200 rpm. Then, the MNPs were centrifuged at 13300 rpm for 15 min at 4 °C. The supernatant was used to evaluate the loading efficiency by measuring the protein concentration with a Micro BCA™ Protein Assay Kit.

2.6. Functionalization of MNPs with IL-4

The steps of the protocol for the functionalization of MNPs with BSA are also on the protocol functionalization of MNPs with IL-4. EDC (20 μL, 43 mM) and of sulfo-NHS (20 μL, 65 mM) were added to a MNPs' suspension (160 μL, 1.25 mg mL^{-1}) in MES (50 mM). The mixture was incubated for 30 min at 37 °C with orbital shaking at 200 rpm. Then, the MNPs were washed twice with water and resuspended in H_2O (180 μL). Later, IL-4 (20 μL, 500 μg μL^{-1}) were added to the MNPs and the mixture was incubated overnight at 37 °C with orbital shaking at 200 rpm. Then, the MNPs were centrifuged at 13300 rpm for 15 min at 4 °C and the supernatant was preserved to analyze the loading efficiency with BCA kit. Finally, the MNPs were washed three times with water and resuspended in cell culture grade water. Loading efficiency of IL-4 on MNPs was evaluated by measuring the protein concentrations in supernatants collected from the previous washing step with a Micro BCA™ Protein Assay Kit.

2.7. Physicochemical characterization of MNPs

The characterization of the crystalline phase of the nanoparticles was performed by powder X-ray diffraction (XRD) using a Philips diffractometer (Panalytical, Callo End, UK) with Cu Kα radiation ($\lambda = 1.5406$ Å). Measurements were collected in the 2θ angle range from 10° to 80° with steps of 0.02° and accounting time of 5 s per step. The peak broadening of XRD patterns is used to obtain crystallite size using Scherrer's equation [41]:

$$d = \frac{k\lambda}{\beta \cos\theta_{hkl}}$$

where d is the mean size of the crystallite (nm), k is the Scherrer constant (0.9, dimensionless), λ is the wavelength of the X-ray beam used (0.154060 nm), β is the full width at half maximum (FWHM, radians) of the peak and θ is the Bragg angle (degrees). The morphology of the MNPs was characterized by transmission electron microscopy (TEM) using a JEOL JEM-1011 microscope (JEOL, Tokyo, Japan) operating at 100 kV. The Fourier transform infrared (FT-IR) spectra were recorded in a Thermo Nicolet Nexus spectrometer (Thermo Fisher Scientific, Madrid, Spain) using the attenuated total reflectance (ATR) method in the range 400–4000 cm^{-1}. Hydrodynamic diameter and zeta potential values of the nanoparticles were measured using a Zetasizer Nano (Malvern, Worcestershire, UK) operating at a wavelength of 633 nm and automatic attenuation at 25 °C. Three different reading were used by the software to calculate all the results. Magnetic properties were assessed by measuring the magnetization curve using a vibrating sample magnetometer (VSM) (DMS, Lowell, MA, USA). The measurements were carried out with an applied field between − 10 and + 10 kOe at room temperature. Thermogravimetric analyses were performed using a TGA Perkin Elmer model 8000 (Perkin, Waltham, MA, USA).

2.8. Cell culture

Human monocytes (THP-1) were cultured in RPMI 1640 supplemented with heat-inactivated fetal bovine serum (FBS, 10 %), antibiotic solution (1 %) and 2-mercaptoethanol (0.05 mM) at 37 °C and 5 % CO_2. Monocytes were differentiated to macrophages by stimulating a cell suspension of 2×10^5 cells mL^{-1} with PMA (Phorbol 12-myristate 13-acetate, 200 nM) for 72 h days. Then, the medium was replaced by fresh medium and cells were cultured for 24 h with standard complete media.

2.9. Toxicity of MNPs

To test the cytotoxicity of the nanoparticle's portfolio macrophages were seeded at a density of 2×10^4 cells $well^{-1}$ in 96-well plates. Nanoparticles were properly diluted in complete cell culture media to reach a final concentration of 0.1, 0.05, 0.01 and 0.001 mg mL^{-1}. Cell monolayers were treated with the nanoparticle suspensions for 24 h. Afterwards, the nanoparticle suspension was removed, cell monolayers were washed twice with DPBS, and WST-1 (15 μL) reagent diluted with culture medium (150 μL) were added to each well. Cells were incubated 2 h and absorbance was read at 450 nm in a microplate reader (Bio-Rad, USA). Cell viability was analyzed relative to control (Milli-Q water diluted as the nanoparticle suspensions) following the equation depicted

below:

$$Cellviability(\%) = \left(\frac{SampleAbsorbance - Blank}{ControlAbsorbance - Blank}\right) \times 100$$

2.10. Macrophage response to MNPs

The effect of SC and MC "per se" on macrophage secretory profile was evaluated on human macrophages. Cells were seeded in 96-well plates at a density of 2 × 104 cells well^{-1} and allowed to attach for 24 h. Afterwards cells were treated with the nanoparticles suspensions at a concentration of 0.4 μg mL^{-1} for 24 h and the macrophage secretome was analyzed in terms of Macrophage Colony-Stimulating Factor (M-CSF), Tumor Necrosis Factor alpha (TNF-α), Interferon gamma (IFN-γ), Interleukin 10 (IL-10) and Interleukin 13 (IL-13) concentration. The concentration of the selected cytokines was quantified by multiplex immunoassay kits (R&D Systems) following the manufacturer's instructions. Samples were diluted 1:1 in assay buffer and loaded into a 96-well plate, after which primary antibodies fixed in magnetic bead suspensions, detection antibodies, and streptavidin–phycoerythrin were added to the samples. The plate was then loaded into a MAGPIX system (Luminex), and analyte concentrations were obtained using the correspondent calibration curve.

2.11. Effect of passive magnetic transfection on M1 macrophages phenotype

Macrophage cells monolayers on 96-well plates were obtained as described in procedure above. Afterwards, cells were treated with IFN-γ (Gibco, USA) at 10 ng mL^{-1} to promote an M1 phenotype macrophage polarization. Stimulated cells were then treated with SC and MC loaded with IL-4 (SCIL-4 and MCIL-4, respectively) using an equivalent IL-4 concentration of 20 ng mL^{-1} that means 0.414 μg mL^{-1} for the SCIL-4 and 0.493 μg mL^{-1} for the MCIL-4. Unstimulated cells, cells without receiving any treatment, cells treated with plain IL-4 at 20 ng mL^{-1} or with the blank SC and MC at the same concentration as IL-4 loaded nanoparticles were used as controls. After 24 h of treatment, cell culture media was removed and stored for cytokine quantification, cells were washed with DPBS and cell viability was evaluated as described for testing the toxicity of the nanoparticles. The secretion of pro-inflammatory and anti-inflammatory cytokines was evaluated as above described besides avoiding the quantification of IFN-γ.

2.12. Magnetotransfection with IL-4 modified MNPs

To perform magnetotransfection, macrophages were seeded in 24-well culture plates at a density of 93,750 cells per well and allowed to attach for 24 h. After stimulation with IFN-γ (10 ng mL^{-1}), the cells were treated with either blank MNPs or with IL-4-loaded NPs at two IL-4 equivalent concentrations 20 and 40 ng mL^{-1} which correspond to 0.41 and 0.82 μg mL^{-1} for SC or 0.49 and 0.98 μg mL^{-1} for MC. The addition of nanoparticles was followed by the placement of a magnet at the bottom of the plate, and the cells were exposed to a magnetic field for one hour in the incubator. Afterwards, the magnet was removed, and cells were allowed to settle for additionally 23 h. The supernatants were collected to quantify the secretion of the selected cytokines, and cell monolayers were processed as described above to assess cell viability. Controls included cells not subjected to the magnetic field, subjected to the magnetic field but not stimulated and subjected to the magnetic field and stimulated. Positive controls consisted of cells stimulated and subjected to the magnetic field and treated with IL-4 at concentrations of 20 ng mL^{-1} and 40 ng mL^{-1}.

3. Results and discussion

3.1. Characterization of citrate coated iron oxide nanoparticles

The powder XRD patterns of SC and MC MNPs are presented in Fig. 1 together with the XRD pattern for magnetite (ICSD card No. 77589).[42] The position and relative intensity of the MNPs diffraction peaks match the main theoretical magnetite reflections, whose diffraction peaks at 18.4, 30.2, 35.6, 37.2, 43.3, 53.7, 57.2, 62.8, 71.3 and 74.4° respond to the [1 1 1], [0 2 2], [1 1 3], [4 2 2], [0 0 4], [2 2 4], [1 1 5], [0 4 4], [0 4 4], [0 2 6] and [3 3 5] planes of cubic Fe_3O_4 lattice, respectively. The results confirm the cubic spinel structure of the nanoparticles, match the data already reported in the literature [43]. From the XRD patterns crystalline size values of 10.9 and 10.3 nm are obtained for SC and MC, respectively.

The morphology of the obtained nanoparticles was examined by transmission electron microscopy (TEM). The analysis of the SC micrograph revealed irregular spherical morphology and a diameter size of about 11 nm (11.0 nm ± 3.0 nm) (Fig. 2**A, B**). The product of MC synthesis consists of uniform spherical particles with diameter size of about 146 nm (145.9 nm ± 35.4 nm) (Fig. 2C, D).

FT-IR spectra of SC and MC are shown in Fig. 3. Both spectra show the same characteristic bands. An absorption band around 562 cm^{-1}, characteristic of the stretching vibrations of the Fe-O bond, indicates the presence of the Fe_3O_4. The adsorption bands appearing at 1379 cm^{-1} and 1576 cm^{-1} are assigned to the symmetric and asymmetric stretching vibrations of carboxylate ions from the citrate on the Fe_3O_4 surface, respectively. In addition, the adsorption bands around 2850 cm^{-1} and 2921 cm^{-1} may be ascribed to the symmetric and asymmetric stretching vibrations of CH_2 group, respectively. The broad adsorption band around 3350 cm^{-1} is attributed to the stretching vibrations of the hydroxyl groups of citrate present on the surface of the nanoparticles, as well as to the traces of molecular water.[44–47] The spectra confirm the success of the coating procedure of the iron oxide nanoparticles with citrate.

The stability of the MNPs was analyzed through the values obtained by dynamic light scattering for the hydrodynamic diameter (D_h), polydispersity index (PDI) and the zeta potential (ζ), shown in Table 1. The hydrodynamic diameter obtained for both SC and MC in aqueous solution (32 and 340 nm, respectively) is larger than the TEM diameter, as it

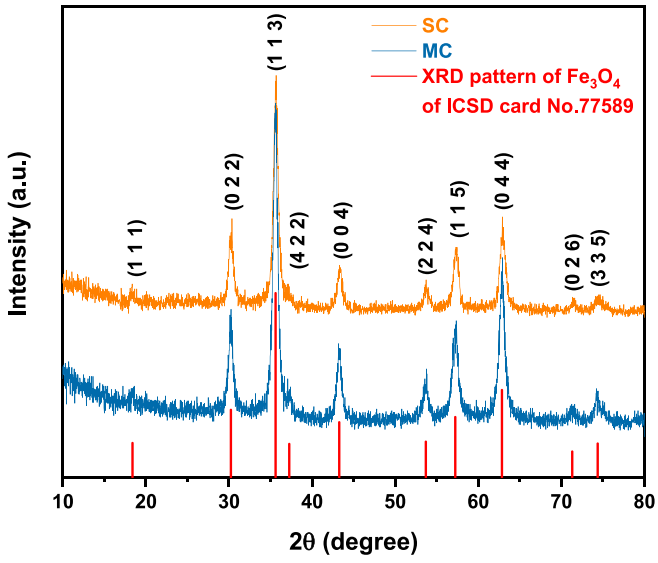

Fig. 1. XRD pattern of magnetite, single-core citrate coated iron oxide nanoparticles (SC) and multi-core citrate coated iron oxide nanoparticles (MC), indicating the diffraction peaks that respond to the planes of cubic Fe_3O_4 lattice.

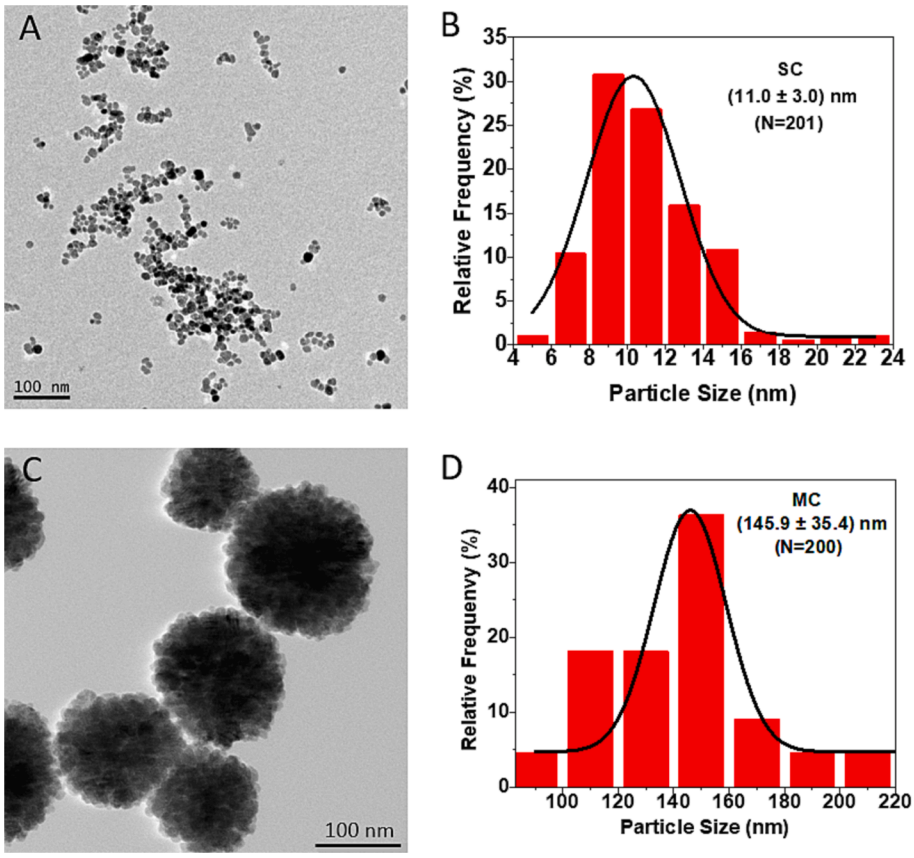

Fig. 2. A) Transmission electron microscopy (TEM) micrograph and (B) size distribution of single-core citrate coated iron oxide nanoparticles (SC). C) TEM micrograph and (D) size distribution of multi-core citrate coated iron oxide nanoparticles (MC). Size distribution was obtained by using the ImageJ software.

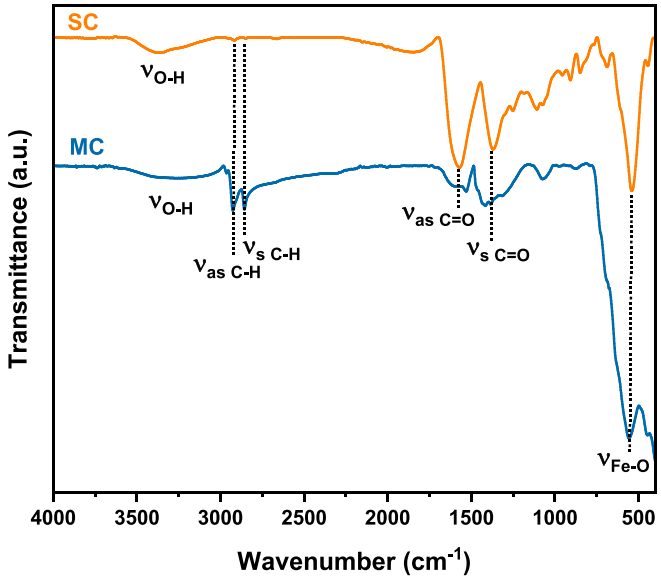

Fig. 3. FT-IR spectra of single-core citrate coated iron oxide nanoparticles (SC) in orange and multi-core citrate coated iron oxide nanoparticles (MC), indicating their characteristic bands. (For interpretation of the references to colour in this figure legend, the reader is referred to the web version of this article.)

can be expected, and already reported for similar systems since this technique analyzes the samples in a wet state and accounts also for the citrate molecules on the MNPs shell and adsorbed water molecules [48]. The obtained PDI values and size distribution of both SC and MC

Table 1
Values of the hydrodynamic radius (D_h), polydispersity index (PDI) and zeta potential obtained for SC and MC in water (w) and complete media (m).

Sample	D_h [nm]	PDI	ζ [mV]
SCw	32 ± 12	0.220	−52 ± 13
MCw	340 ± 218	0.233	−51 ± 11
SCm	85 ± 33	0.224	–
MCm	174 ± 218	0.136	–

nanoparticles (0.220 and 0.233, respectively) are correlated with single nanoparticle population. The highly negative zeta potential, around − 50 mV in both cases, indicates the moderate electrostatic stability of the nanoparticles in aqueous suspension [49]. Moreover, when the nanoparticles were diluted in complete cell culture media at the treatment concentrations (0.4 μg mL^{-1}) SC nanoparticles suspensions showed an increase in hydrodynamic diameter while maintaining a similar PDI. On the other hand, no effect was observed for MC. The increase in size of SC could be correlated with the adsorption of the media proteins on the nanoparticles surface forming a corona that could lead to small nanoparticle aggregates.

Magnetic properties of MNPs were investigated by measuring their magnetization curves with a vibrating sample magnetometer (VSM) at room temperature over a range of magnetic fields from − 10 kOe and + 10 kOe where the magnetization data were normalized to the content of magnetic mass of each sample. Fig. 4 shows the magnetic hysteresis loops of SC and MC from which relevant parameters such as saturation magnetization (M_S), remanence (M_R) or coercive force (H_C), compiled in Table 2, can be obtained. The saturation magnetization values revealed to be similar in both MNPs, 68 emu/g for SC and 67 emu/g for MC which are in good agreement with the data from the literature [44,50] and

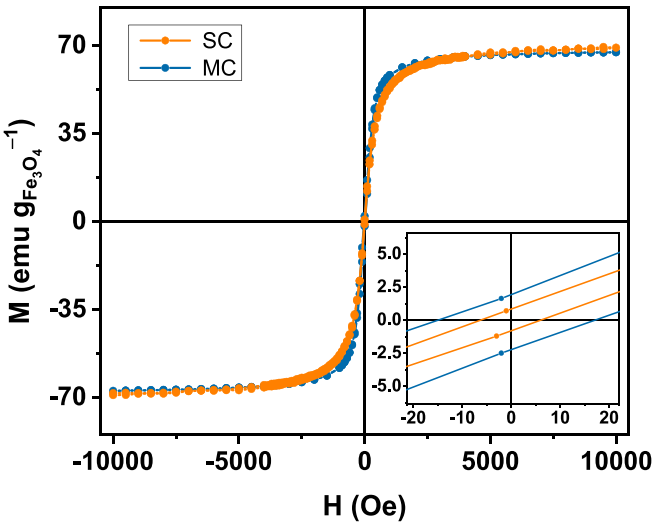

Fig. 4. Magnetic hysteresis loops of single-core citrate coated iron oxide nanoparticles (SC) and multi-core citrate coated iron oxide nanoparticles (MC) at room temperature showing superparamagnetic properties. Inset: Scale amplification of hysteresis loops.

Table 2
The values of saturation magnetization (M_S), remanence (M_R), and coercive force (H_C) for the SC and MC magnetic nanoparticles were determined through the analysis of their respective hysteresis loops.

Sample	M_S [emu/g]	M_R [emu/g]	H_C [Oe]
SC	68.7	0.8	6.1
MC	67.3	2.1	16.1

lower than the values of bulk magnetite (M_S = 92 emu/g) [51], due to the presence of a dead magnetic layer in the surface of small magnetic nanoparticles that reduces the magnetization [52]. Despite the notable differences in the overall sizes of the MNPs, 11 nm and 146 nm for SC and MC, respectively, the M_S obtained is similar agreeing with the crystalline size values (10.9 and 10.3 nm for SC and MC, respectively) and demonstrating that MC are formed by the clustering of smaller MNPs. On the other hand, the observed negligible coercive force (6.1 and 16.1 Oe) and remanence magnetization (0.8 and 2.1 emu/g) for SC and MC, respectively, suggest a superparamagnetic behavior of the MNPs [53].

3.2. Loading of MNPs with BSA and IL-4

Previously to MNPs loading with IL-4, several tests were performed with BSA to determine the optimum loading procedure. Loading efficiencies of BSA and IL-4 on MNPs were analyzed by quantifying the non-incorporated protein in the supernatants with a Micro BCA™ Protein Assay Kit.

A first approach by electrostatic adsorption of BSA on the surface of MNPs was tried, showing and adsorption efficiency below 50 % in both SC and MC (Fig. 5), that could not be enhanced by testing longer incubation times (on the contrary, it even significantly reduced the adsorption in the case of MC).

Then, a chemical bonding strategy was essayed to achieve a better BSA loading performance following the well-known EDC-NHS activation route (see description in experimental section). The efficiency of the chemical bonding raised to 92 % for BSA loading of SC MNPs and 62 % for BSA loading of MC MNPs, showing a remarkable improvement on the loading capacity of the MNPs. Once the loading procedure was optimized using BSA, the same conditions were applied for an efficient loading of IL-4 onto the SC and MC MNPs. We observed that, the loading

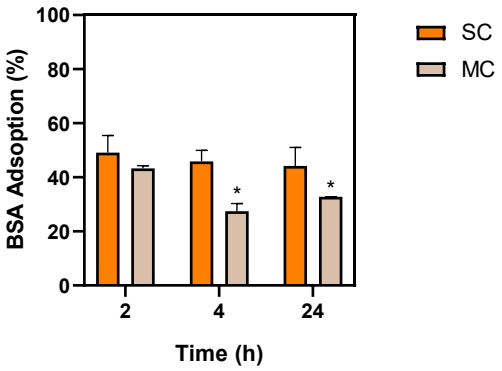

Fig. 5. BSA adsorption into single-core and multi-core iron oxide nanoparticles by electrostatic interactions at times 2, 4 and 24 h. * Denotes statistically significant differences with SC at the correspondent time-point ($p < 0.05$).

efficiency was maintained for SCIL-4 with a 93 % while for MCIL-4, the loading increased significantly up to an 81 %. The higher loading efficiency for the SC can be justified by the smaller size of the nanoparticles, that is related to the surface-to-volume ratio in the nanoscale [54]. Smaller MNPs present higher surface area ratio, and considering that for the same mass, the number of MNPs is larger in the case of SC, there is a larger surface area available for the functionalization. In addition, the curvature of the MNPs surface, which depends on the size of the nanoparticles, can significantly affect the loading with cytokines [55].

The FT-IR spectra of IL-4 loaded SC (SCIL-4) and IL-4 loaded MC (MCIL–4) shown in Fig. 6 corroborates the success of the functionalization. The absorption bands that were previously assigned to Fe-O bond, COO^- and CH_2 groups in the citrate coated iron oxide nanoparticles remain in the spectra of the loaded MNPs, together with an absorption band at 1652 cm^{-1} corresponding to the characteristic amide I band of proteins, showing that IL-4 was successfully linked to the nanoparticles [56,57]. This is also confirmed by the absence of the band corresponding to the stretching vibrations of hydroxyl groups present on the surface of SC and MC.

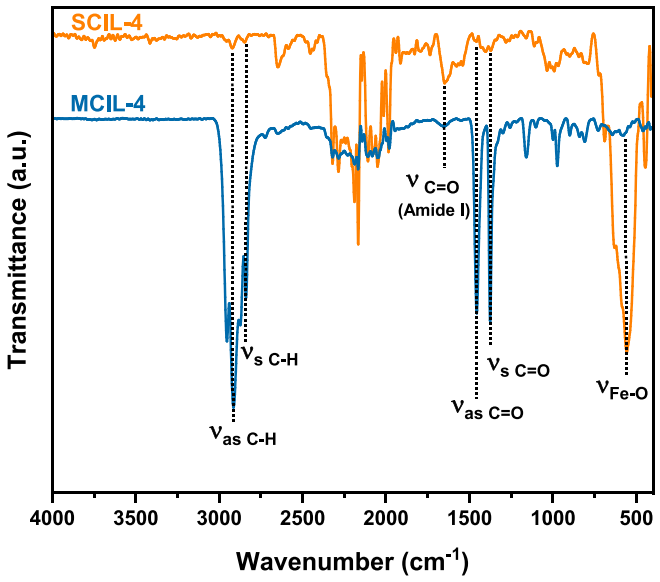

Fig. 6. FT-IR spectra of IL-4 loaded SC (SCIL-4) in purple and IL-4 loaded MC (MCIL-4) in red, indicating their characteristic bands. (For interpretation of the references to colour in this figure legend, the reader is referred to the web version of this article.)

3.3. Macrophage response to MNPs

3.3.1. Effect of MNPs on non-polarized macrophages

Macrophages are phagocytic highly plastic cells that play crucial roles in inflammation and tissue homeostasis. Associated to their phagocytic ability, these cells have been previously reported to highly uptake magnetic nanoparticles, serving as macrophage labeling agents [58]. This behavior could led to toxic effects at the cell level and changes in macrophage phenotype. To corroborate the lack of toxicity and any unexpected shift in macrophage phenotype, THP1-derived macrophages were treated with citrate coated single (SC) and multi-core (MC) iron oxide nanoparticle suspensions. Afterwards, cell viability and macrophage cytokine fingerprints were determined by measuring the secretion of M1 and M2 associated cytokines.

As shown in Fig. 7, the treatment with un-loaded iron oxide nanoparticles did not cause a detrimental effect in cell viability and no changes in the cytokine secretion were observed for the tested conditions compared to control. In agreement with our findings the treatment with iron oxide nanoparticles have been previously reported to not modify macrophage proliferation and polarization capacity while not inducing cytokine production [59,60].

3.3.2. Effect of IL-4 loaded MNPs on M1 macrophages

Fig. 8 shows the cytokine secretion of interferon-gamma stimulated macrophages, M1 phenotype, treated with both un-loaded and IL-4 loaded iron oxide nanoparticles. In this scenario, clear differences can be observed between cells treated with single or multicore nanoparticles. Cells treated with SC nanoparticles loaded with IL-4 showed a decrease in the secretion of M-CSF and TNF-α when compared to non-treated M1 macrophages, similarly to those results obtained with IL-4 alone showing the expected anti-inflammatory effect. On the contrary, the secretion of these cytokines was significantly increased in cells treated with IL-4 loaded MC compared to non-treated M1. The incorporation of IL-4 to MC nanoparticles promoted a decreased of M-CSF and TNF-α secretion compared to cells treated with plain MC indicating that the cytokine maintains its activity. However, these values remained higher than non-treated M1 macrophages, this effect, derived from the treatment with MC nanoparticles, is not related to cell toxicity as the metabolic activity of the treated cells were similar for all the conditions except for IL-4 that slightly promoted the cell metabolic activity of M1 macrophages.

Some authors have hypothesized the capacity of iron oxide nanoparticles to control M2/M1 macrophage phenotype switch in tumor settings and overall macrophage behaviors. This effect has been thought to be related to the presence of iron inside the macrophages that may modulate the macrophage polarization status by controlling the expression of transferrin and other iron transport-related proteins [61]. However, this effect has been previously described to be dependent on the iron oxide concentration [62]. Interestingly, while on Fig. 7 we show the lack of cell response after the treatment with all the MNPs, the opposite effect is observed when cells are stimulated with interferon-gamma (Fig. 8) despite using the same nanoparticle concentration for both studies. Therefore, the differences in cell behavior observed between both settings would be attributed to the polarization stage of macrophages, un-polarized macrophages (Fig. 7) versus M1 (IFN-γ stimulated cells) macrophages (Fig. 8). The role of iron on the polarization of macrophages is quite controversial with non-consistent data regarding their effect as anti-inflammatory or pro-inflammatory inductor on the different stages of macrophages [63]. Some authors point out iron supplementation in vivo led to M1 polarization and TNF-α secretion of resting macrophages through the increased expression of mitogen-activated protein kinase (MAPK) [64]. On the other hand, other authors have pointed out that M1 macrophages subjected to an in vitro iron stimulation at a concentration of 25 μg mL^{-1} decreased the expression of IL-6, IL-1β and TNF-α [65]. In this work, for the first time we reported that macrophages treated with low concentrations of iron oxide nanoparticles behave differently depending on the polarization stage independently of the concentration of iron. This fact may be related to the different roles in iron homeostasis of macrophages depending on the polarization stage. It has been reported that M1 macrophages tend to accumulate iron inside the cells to act as a bacteriostatic element by increasing the expression of ferritin, however, M2 macrophages are characterized by iron secretion [66]. This ability of M1 macrophages to retain iron inside the cells could explain the increase in TNF-α production observed in M1 treated macrophages even with low nanoparticle concentration. Moreover, we also found this effect is related to particle size and morphology since the inclusion of IL-4 in the nanoparticles was able to significantly reduce the secretion of TNF-α only for SC nanoparticles.

3.3.3. Magnetotransfection with IL-4 modified MNPs

As a step forward on analyzing the response of macrophages to iron oxide nanoparticles we took advantage of the capacity of these nanoparticles to respond to magnetic fields. M1 macrophages were magnetotransfected with SC and MC at two concentrations, the one previously used, equivalent to IL-4 concentration 20 ng mL^{-1}, and the double equivalent IL-4 concentration 40 ng mL^{-1}. As shown in supplementary Fig. 1**S**, the presence of the magnet itself increased the secretion of pro-inflammatory cytokines. The ability of macrophages to respond to magnetic fields has been previously reported being able to control cell elongation and polarization [67]. In this scenario, the treatment with IL-4 at 20 ng mL^{-1} either alone or loaded into the nanoparticles did not produce any effect on the cytokine secretion (Fig. 9**A**). However, the treatment of the cells with both SC and MC led to an increase expression in M-CSF and TNF-α suggesting further activation of the cells. On the other hand, when the concentration was increased the treatment with

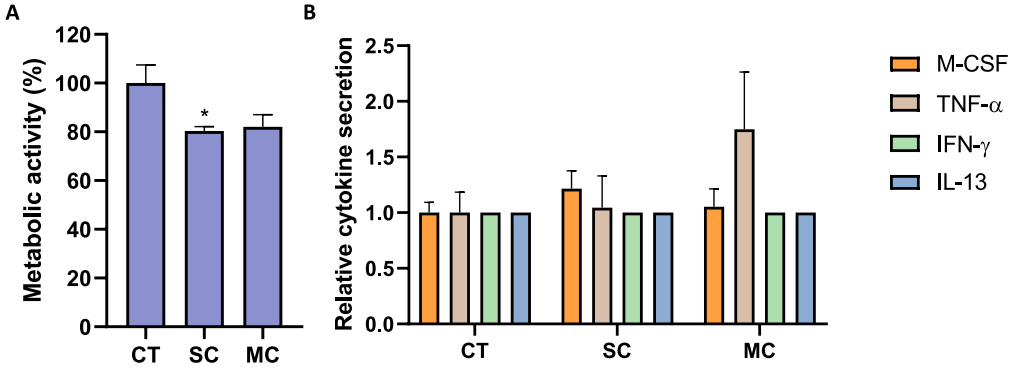

Fig. 7. A) Cell viability of un-stimulated macrophages after 24 h of treatment with single (0.26 μg mL^{-1} of iron) or multi-core nanoparticles (0.28 μg mL^{-1} of iron); B) Cytokine secretion of un-stimulate cells treated with the iron oxide nanoparticles at the same concentration. CT stands for control, SC stands for single core, MC stands for multicore. * Denotes statistically significant values compared to control $p < 0.05$.

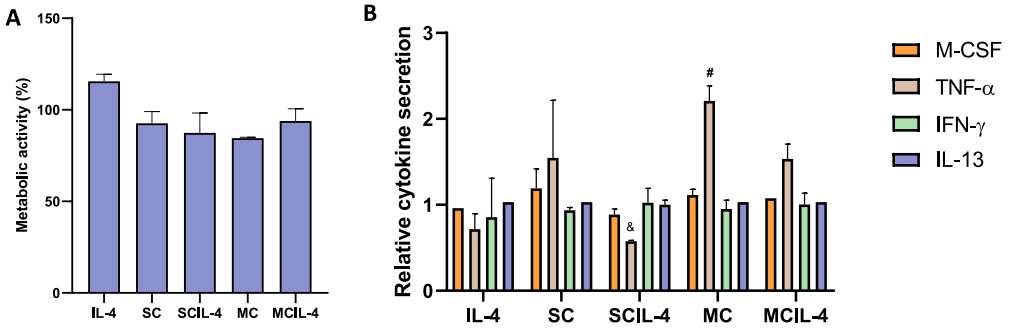

Fig. 8. A) Cell viability of stimulated macrophages after 24 h of treatment with single (0.26 μg mL^{-1} of iron) or multi-core nanoparticles (0.28 μg mL^{-1} of iron) unloaded or including IL-4 at an equivalent IL-4 concentration of 20 ng mL^{-1}; B) Cytokine secretion of stimulate cells treated with the iron oxide nanoparticles at the same concentration. CT stands for control, SC stands for single core, MC stands for multicore. & Denotes statistically significant values compared to cells treated with single core nanoparticles (SC); # Denotes statistically significant values compared to cells treated with IL-4 loaded single core nanoparticles (SCIL-4) $p < 0.05$.

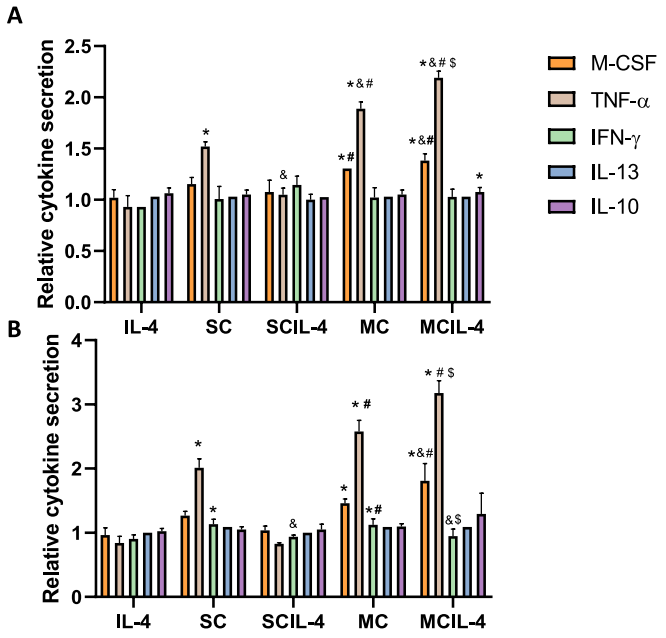

Fig. 9. A) Cytokine secretion of stimulate cells treated with the iron oxide nanoparticles at the same concentration after 24 h of treatment with single (0.26 μg mL^{-1} of iron) or multi-core nanoparticles (0.28 μg mL^{-1} of iron) unloaded or including IL-4 at an equivalent IL-4 concentration of 20 ng mL^{-1}; B) Cytokine secretion of stimulate cells treated with the iron oxide nanoparticles at the same concentration after 24 h of treatment with single (0.52 μg mL^{-1} of iron) or multi-core nanoparticles (0.56 μg mL^{-1} of iron) un-loaded or including IL-4 at an equivalent IL-4 concentration of 40 ng mL^{-1}. * Denotes statistically significant values compared to cells treated with IL-4; & Denotes statistically significant values compared to cells treated with single core nanoparticles (SC); # Denotes statistically significant values compared to cells treated with IL-4 loaded single core nanoparticles (SCIL-4); $ Denotes statistically significant values compared to cells treated with multi core nanoparticles (MC) $p < 0.05$.

IL-4 efficiently decreased the secretion of the pro-inflammatory cytokine TNF-α obtaining a similar result for SCIL-4 treated cells. On the contrary the treatment with SC, MC and MCIL-4 led to a further increase in M-CSF and TNF-α. These data corroborate the hypothesis that the cell behavior to iron nanoparticles is dependent on the morphology and shape of the nanoparticles and on the activation stage of the cells. In agreement with this, some authors have stated that bigger iron oxide nanoparticles (≈ 30 nm) are able to induce a higher responses to macrophages than smaller ones (≈ 10 nm) increasing the secretion of TNF-α and IL-6 in naïve macrophages [68]. Conversely, Chen and coworkers found that small SPIONs (≈ 30 nm) led to higher IL-1β secretion than higher ones (≈ 120 nm) in both naïve macrophages and M1 macrophages [69]. On the other hand, other authors state the treatment of THP 1-derived macrophages with SPIONS of around 80 nm at 20 and 50 μM Fe did not change the cytokine profile of naïve macrophages [70]. Taking together, the data available in the literature is not consistent for either nanoparticle size and concentration. These results could be explained by the different stage of the macrophages that has been proven to condition cell response.

Considering the relevance of macrophages on tissue homeostasis and tumor control, designing nanoparticles able to exert the desired effect on the macrophages is crucial. This step would need to consider the polarization stage of the cells as it will condition the therapeutic response. Based on the obtained data, SCIL-4 MNPs without magnetotransfection seem the best ones for tissue regeneration purposes while MCIL-4 MNPs seem to be more promising for tumor control.

4. Conclusions

Citrate coated single-core and multi-core iron oxide nanoparticles were successfully loaded with IL-4 through chemical bonding. The absence of toxicity was corroborated by treating THP-1 derived macrophages with the mentioned nanoparticles. A lack of cell response was observed after the treatment of un-polarized macrophages (M0) with single-core and multi-core iron oxide nanoparticles. However, the treatment of INF- γ stimulated macrophages (M1) with the same concentration of iron oxide nanoparticles, induces a pro-inflammatory response in the case of multi-core NPs. Therefore, in this work, for the first time we reported that macrophages treated with low concentrations of iron oxide nanoparticles behave differently depending on the polarization stage independently of the concentration of iron. Furthermore, the size and morphology of the nanoparticles determines the effect of the IL-4 loaded MNPs on M1 macrophages. The studied IL-4 loaded SC MNPs favored the polarization of M1 macrophages towards M2 phenotype, while IL-4 loaded MC MNPs further stimulated the M1 phenotype.

CRediT authorship contribution statement

Ángela Arnosa-Prieto: Methodology, Investigation, Writing – review & editing. **Patricia Diaz-Rodriguez:** Conceptualization, Methodology, Investigation, Writing – review & editing, Supervision. **Manuel A. González-Gómez:** Investigation. **Pelayo García-Acevedo:** Investigation. **Lisandra de Castro-Alves:** Investigation. **Yolanda Piñeiro:** Conceptualization, Writing – review & editing, Supervision. **José Rivas:** Conceptualization, Writing – review & editing, Supervision.

Declaration of Competing Interest

The authors declare that they have no known competing financial interests or personal relationships that could have appeared to influence the work reported in this paper.

Data availability

Data will be made available on request.

Acknowledgments

This work was supported by the Programa de Axudas de apoio á etapa predoutoral 2020 of Xunta de Galicia, by the European Commission under the BOW project (FETPROACT-EIC-05-2019, Grant 952183), CARTsol project (PLEC2022-009217 funded by MICINN/AEI /10.13039/501100011033 and NextGenerationEU/ PRTR) and partially supported by the Spanish Ministry of Science and Innovation (ref PID2020-112626RB-C21), Modalities «Research Challenges» and «Knowledge Generation» and the Regional Consellería de Innovación Program for the Grupos de Referencia Competitiva 2021 —GRC2021 project of Xunta de Galicia.

Appendix A. Supplementary material

Supplementary data to this article can be found online at https://doi.org/10.1016/j.jcis.2023.11.004.

References

[1] A. Shapouri-Moghaddam, S. Mohammadian, H. Vazini, M. Taghadosi, S. A. Esmaeili, F. Mardani, B. Seifi, A. Mohammadi, J.T. Afshari, A. Sahebkar, Macrophage plasticity, polarization, and function in health and disease, J. Cell. Physiol. 233 (2018) 6425–6440, https://doi.org/10.1002/jcp.26429.

[2] T.L. Fernandes, A.H. Gomoll, C. Lattermann, A.J. Hernandez, D.F. Bueno, M. T. Amano, Macrophage: a potential target on cartilage regeneration, Front. Immunol. 11 (2020) 1–9, https://doi.org/10.3389/fimmu.2020.00111.

[3] J. Dort, P. Fabre, T. Molina, N.A. Dumont, Macrophages are key regulators of stem cells during skeletal muscle regeneration and diseases, Stem Cells Int. 2019 (2019), https://doi.org/10.1155/2019/4761427.

[4] L. xun Wang, S. xi Zhang, H. juan Wu, X. lu Rong, J. Guo, M2b macrophage polarization and its roles in diseases, J. Leukoc. Biol. 106 (2019) 345–358. https://doi.org/10.1002/JLB.3RU1018-378RR.

[5] Y. Xie, C. Hu, Y. Feng, D. Li, T. Ai, Y. Huang, X. Chen, L. Huang, J. Tan, Osteoimmunomodulatory effects of biomaterial modification strategies on macrophage polarization and bone regeneration, Regen. Biomater. 7 (2020) 233–245, https://doi.org/10.1093/rb/rbaa006.

[6] W. Zhang, F. Zhao, D. Huang, X. Fu, X. Li, X. Chen, Strontium-substituted submicrometer bioactive glasses modulate macrophage responses for improved bone regeneration, ACS Appl. Mater. Interfaces. 8 (2016) 30747–30758, https://doi.org/10.1021/acsami.6b10378.

[7] T.A. Wynn, K.M. Vannella, Macrophages in tissue repair, regeneration, and fibrosis, Immunity 44 (2016) 450–462, https://doi.org/10.1016/j.immuni.2016.02.015.

[8] Y. Niu, Z. Wang, Y. Shi, L. Dong, C. Wang, Modulating macrophage activities to promote endogenous bone regeneration: biological mechanisms and engineering approaches, Bioact. Mater. 6 (2021) 244–261, https://doi.org/10.1016/j.bioactmat.2020.08.012.

[9] X. Guo, J. Bai, G. Ge, Z. Wang, Q. Wang, K. Zheng, H. Tao, L. Zhang, H. Zhang, D. Wang, X. Zhang, H. Li, G. Pan, D. Geng, Bioinspired peptide adhesion on Ti implants alleviates wear particle-induced inflammation and improves interfacial osteogenesis, J. Colloid Interface Sci. 605 (2022) 410–424, https://doi.org/10.1016/j.jcis.2021.07.079.

[10] C. Schlundt, H. Fischer, C.H. Bucher, C. Rendenbach, G.N. Duda, K. Schmidt-Bleek, The multifaceted roles of macrophages in bone regeneration: a story of polarization, activation and time, Acta Biomater. 133 (2021) 46–57, https://doi.org/10.1016/j.actbio.2021.04.052.

[11] K. Schmidt-Bleek, H. Schell, J. Lienau, N. Schulz, P. Hoff, M. Pfaff, G. Schmidt, C. Martin, C. Perka, F. Buttgereit, H.D. Volk, G. Duda, Initial immune reaction and angiogenesis in bone healing, J. Tissue Eng. Regen. Med. 8 (2014) 120–130, https://doi.org/10.1002/term.1505.

[12] R.L.Y. Shin, C.W. Lee, O.Y.J. Shen, H. Xu, O.K.S. Lee, The crosstalk between mesenchymal stem cells and macrophages in bone regeneration: a systematic review, Stem Cells Int. 2021 (2021), https://doi.org/10.1155/2021/8835156.

[13] J. Kowal, M. Kornete, J.A. Joyce, Re-education of macrophages as a therapeutic strategy in cancer, Immunotherapy. 11 (2019) 677–689, https://doi.org/10.2217/imt-2018-0156.

[14] L. Xu, X. Xie, Y. Luo, The role of macrophage in regulating tumour microenvironment and the strategies for reprogramming tumour-associated macrophages in antitumour therapy, Eur. J. Cell Biol. 100 (2021), 151153, https://doi.org/10.1016/j.ejcb.2021.151153.

[15] M.A.F. Yahaya, M.A.M. Lila, S. Ismail, M. Zainol, N.A.R.N.M. Afizan, Tumour-Associated Macrophages (TAMs) in colon cancer and how to reeducate them, J Immunol. Res. 2019 (2019), https://doi.org/10.1155/2019/2368249.

[16] K. Li, L. Lu, C. Xue, J. Liu, Y. He, J. Zhou, Z. Xia, L. Dai, Z. Luo, Y. Mao, K. Cai, Polarization of tumor-associated macrophage phenotype: Via porous hollow iron nanoparticles for tumor immunotherapy in vivo, Nanoscale. 12 (2020) 130–144, https://doi.org/10.1039/c9nr06505a.

[17] S. Han, W. Wang, S. Wang, S. Wang, R. Ju, Z. Pan, T. Yang, G. Zhang, H. Wang, L. Wang, Multifunctional biomimetic nanoparticles loading baicalin for polarizing tumor-associated macrophages, Nanoscale. 11 (2019) 20206–20220, https://doi.org/10.1039/c9nr03353j.

[18] L. Hou, X. Gong, J. Yang, H. Zhang, W. Yang, X. Chen, Hybrid-membrane-decorated prussian blue for effective cancer immunotherapy via tumor-associated macrophages polarization and hypoxia relief, Adv. Mater. 34 (2022) 1–11, https://doi.org/10.1002/adma.202200389.

[19] Y. Wei, Z. Wang, J. Yang, R. Xu, H. Deng, S. Ma, T. Fang, J. Zhang, Q. Shen, Reactive oxygen species / photothermal therapy dual-triggered biomimetic gold nanocages nanoplatform for combination cancer therapy via ferroptosis and tumor-associated macrophage repolarization mechanism, J. Colloid Interface Sci. 606 (2022) 1950–1965, https://doi.org/10.1016/j.jcis.2021.09.160.

[20] J. Lee, H. Byun, S.K. Madhurakkat Perikamana, S. Lee, H. Shin, Current advances in immunomodulatory biomaterials for bone regeneration, Adv. Healthc. Mater. 8 (2019), https://doi.org/10.1002/adhm.201801106.

[21] A.J. Boutilier, S.F. Elsawa, Macrophage polarization states in the tumor microenvironment, Int. J. Mol. Sci. 22 (2021), https://doi.org/10.3390/ijms22136995.

[22] G. Sun, S. Yang, H. Cai, Y. Shu, Q. Han, B. Wang, Z. Li, L. Zhou, Q. Gao, Z. Yin, Molybdenum disulfide nanoflowers mediated anti-inflammation macrophage modulation for spinal cord injury treatment, J. Colloid Interface Sci. 549 (2019) 50–62, https://doi.org/10.1016/j.jcis.2019.04.047.

[23] G. Pellizzari, C. Hoskin, S. Crescioli, S. Mele, J. Gotovina, G. Chiaruttini, R. Bianchini, K. Ilieva, H.J. Bax, S. Papa, K.E. Lacy, E. Jensen-Jarolim, S. Tsoka, D. H. Josephs, J.F. Spicer, S.N. Karagiannis, IgE re-programs alternatively-activated human macrophages towards pro-inflammatory anti-tumoural states, EBioMedicine. 43 (2019) 67–81, https://doi.org/10.1016/j.ebiom.2019.03.080.

[24] G. Hu, Y. Su, B.H. Kang, Z. Fan, T. Dong, D.R. Brown, J. Cheah, K.D. Wittrup, J. Chen, High-throughput phenotypic screen and transcriptional analysis identify new compounds and targets for macrophage reprogramming, Nat. Commun. 12 (2021) 1–14, https://doi.org/10.1038/s41467-021-21066-x.

[25] A. Roghanian, G. Hu, C. Fraser, M. Singh, R.B. Foxall, M.J. Meyer, E. Lees, H. Huet, M.J. Glennie, S.A. Beers, S.H. Lim, M. Ashton-Key, S.M. Thirdborough, M.S. Cragg, J. Chen, Cyclophosphamide enhances cancer antibody immunotherapy in the resistant bone marrow niche by modulating macrophage FcγR expression, Can. Immunol. Res. 7 (2019) 1876–1890, https://doi.org/10.1158/2326-6066.CIR-18-0835.

[26] J. Nakamura, S. Watanabe, H. Kimura, M. Kobayashi, T. Karasawa, R. Kamata, F. Usui-Kawanishi, A. Sadatomo, H. Mizukami, N. Nagi-Miura, N. Ohno, T. Kasahara, S. Minota, M. Takahashi, Adeno-associated virus vector-mediated interleukin-10 induction prevents vascular inflammation in a murine model of kawasaki disease /631/443/592/75 /692/4019/592 /13 /13/21 /42 /42/44 /13/51 /13/106 /13/95 /38 article, Sci. Rep. 8 (2018) 1–13, https://doi.org/10.1038/s41598-018-25856-0.

[27] A. Annoni, S. Gregori, L. Naldini, A. Cantore, Modulation of immune responses in lentiviral vector-mediated gene transfer, Cell. Immunol. 342 (2019), 103802, https://doi.org/10.1016/j.cellimm.2018.04.012.

[28] H.M. Viecelli, R.P. Harbottle, S.P. Wong, A. Schlegel, M.K. Chuah, T. Vandendriessche, C.O. Harding, B. Thöny, Treatment of phenylketonuria using minicircle-based naked-DNA gene transfer to murine liver, Hepatology. 60 (2014) 1035–1043, https://doi.org/10.1002/hep.27104.

[29] Y. Jiang, J. Hardie, Y. Liu, M. Ray, X. Luo, R. Das, R.F. Landis, M.E. Farkas, V. M. Rotello, Nanocapsule-mediated cytosolic siRNA delivery for anti-inflammatory treatment, J. Control. Release. 283 (2018) 235–240, https://doi.org/10.1016/j.jconrel.2018.06.001.

[30] M.A. Shahbazi, M. Sedighi, T. Bauleth-Ramos, K. Kant, A. Correia, N. Poursina, B. Sarmento, J. Hirvonen, H.A. Santos, Targeted reinforcement of macrophage reprogramming toward M2 polarization by IL-4-Loaded hyaluronic acid particles, ACS Omega. 3 (2018) 18444–18455, https://doi.org/10.1021/acsomega.8b03182.

[31] L. Wang, H. Zhang, L. Sun, W. Gao, Y. Xiong, A. Ma, X. Liu, L. Shen, Q. Li, H. Yang, Manipulation of macrophage polarization by peptide-coated gold nanoparticles and its protective effects on acute lung injury, J. Nanobiotechnology. 18 (2020) 1–16, https://doi.org/10.1186/s12951-020-00593-7.

[32] L.L. Israel, A. Galstyan, E. Holler, J.Y. Ljubimova, Magnetic iron oxide nanoparticles for imaging, targeting and treatment of primary and metastatic tumors of the brain, J. Control. Release. 320 (2020) 45–62, https://doi.org/10.1016/j.jconrel.2020.01.009.

[33] M. Li, J. Bao, J. Zeng, L. Huo, X. Shan, X. Cheng, D. Qiu, W. Miao, X. Zhu, G. Huang, K. Ni, Z. Zhao, Engineering manganese ferrite shell on iron oxide nanoparticles for enhanced T1 magnetic resonance imaging, J. Colloid Interface Sci. 626 (2022) 364–373, https://doi.org/10.1016/j.jcis.2022.06.118.

[34] N. Xiao, W. Gu, H. Wang, Y. Deng, X. Shi, L. Ye, T1–T2 dual-modal MRI of brain gliomas using PEGylated Gd-doped iron oxide nanoparticles, J. Colloid Interface Sci. 417 (2014) 159–165, https://doi.org/10.1016/j.jcis.2013.11.020.

[35] Y. Piñeiro, M.A. González Gómez, L. de Castro Alves, A. Arnosa Prieto, P. García Acevedo, R.S. Gudiña, J. Puig, C. Teijeiro, S. Yáñez Vilar, J. Rivas, Hybrid nanostructured magnetite nanoparticles: From bio-detection and theragnostics to regenerative medicine, Magnetochemistry. 6 (2020) 4, https://doi.org/10.3390/magnetochemistry6010004.
[36] J. Sharkey, P.J. Starkey Lewis, M. Barrow, S.M. Alwahsh, J. Noble, E. Livingstone, R.J. Lennen, M.A. Jansen, J.G. Carrion, N. Liptrott, S. Forbes, D.J. Adams, A. E. Chadwick, S.J. Forbes, P. Murray, M.J. Rosseinsky, C.E. Goldring, B.K. Park, Functionalized superparamagnetic iron oxide nanoparticles provide highly efficient iron-labeling in macrophages for magnetic resonance–based detection in vivo, Cytotherapy. 19 (2017) 555–569, https://doi.org/10.1016/j.jcyt.2017.01.003.
[37] S. Zanganeh, G. Hutter, R. Spitler, O. Lenkov, M. Mahmoudi, A. Shaw, J. S. Pajarinen, H. Nejadnik, S. Goodman, M. Moseley, L.M. Coussens, H.E. Daldrup-Link, Iron oxide nanoparticles inhibit tumour growth by inducing pro-inflammatory macrophage polarization in tumour tissues, Nat. Nanotechnol. 11 (2016) 986–994, https://doi.org/10.1038/nnano.2016.168.
[38] D. Deng, S. Fu, Z. Cai, X. Fu, R. Jin, H. Ai, Surface carboxylation of iron oxide nanoparticles brings reduced macrophage inflammatory response through inhibiting macrophage autophagy, Regen. Biomater. 9 (2022), https://doi.org/10.1093/rb/rbac018.
[39] X. Jiang, F. Wang, W. Cai, X. Zhang, Trisodium citrate-assisted synthesis of highly water-dispersible and superparamagnetic mesoporous Fe3O4 hollow microspheres via solvothermal process, J. Alloys Compd. 636 (2015) 34–39, https://doi.org/10.1016/j.jallcom.2015.02.156.
[40] S. Puertas, P. Batalla, M. Moros, E. Polo, P. Pino, J.M. Guisán, V. Grazú, J.M. de la Fuente, Taking Advantage of Unspecific Interactions to Produce Highly Active Conjugates, ACS Nano. 5 (2011) 4521–4528, https://doi.org/10.1021/nn200019s.
[41] P. Scherrer, Nachrichten von der Gesellschaft der Wissenschaften zu Göttingen, Math. Klasse. 2 (1918) 98–100.
[42] A.M. Finger, L.W. Hazen, R.M. Hofmeister, High-pressure crystal chemistry of spinel (MgAl2O4) and magnetite (Fe3O4): comparisons with silicate spinels, Phys. Chem. Miner. 13 (1986) 215–220.
[43] J. Mürbe, A. Rechtenbach, J. Töpfer, Synthesis and physical characterization of magnetite nanoparticles for biomedical applications, Mater. Chem. Phys. 110 (2008) 426–433, https://doi.org/10.1016/j.matchemphys.2008.02.037.
[44] C. Hui, C. Shen, T. Yang, L. Bao, J. Tian, H. Ding, C. Li, H.J. Gao, Large-scale Fe3O4 nanoparticles soluble in water synthesized by a facile method, J. Phys. Chem. c. 112 (2008) 11336–11339, https://doi.org/10.1021/jp801632p.
[45] A. Qureashi, A.H. Pandith, A. Bashir, T. Manzoor, L.A. Malik, F.A. Sheikh, Citrate coated magnetite: a complete magneto dielectric, electrochemical and DFT study for detection and removal of heavy metal ions, Surfaces and Interfaces. 23 (2021), 101004, https://doi.org/10.1016/j.surfin.2021.101004.
[46] S. Nigam, K.C. Barick, D. Bahadur, Development of citrate-stabilized Fe3O4 nanoparticles: conjugation and release of doxorubicin for therapeutic applications, J. Magn. Magn. Mater. 323 (2011) 237–243, https://doi.org/10.1016/j.jmmm.2010.09.009.
[47] Y. Na, S. Yang, S. Lee, Evaluation of citrate-coated magnetic nanoparticles as draw solute for forward osmosis, Desalination. 347 (2014) 34–42, https://doi.org/10.1016/j.desal.2014.04.032.
[48] L. Jitkang, Y.S. Pin, C.H. Xin, L.S. Chun, Characterization of magnetic nanoparticle by dynamic light scattering, Nanoscale Res. Lett. 8 (2013) 308–381. www.nanoscalereslett.com/content/8/1/381.
[49] O.Z. Sharaf, R.A. Taylor, E. Abu-Nada, On the colloidal and chemical stability of solar nanofluids: From nanoscale interactions to recent advances, Phys. Rep. 867 (2020) 1–84, https://doi.org/10.1016/j.physrep.2020.04.005.
[50] S. Sun, H. Zeng, D.B. Robinson, S. Raoux, P.M. Rice, S.X. Wang, G. Li, Monodisperse MFe2O4 (M = Fe Co, Mn) nanoparticles, J. Am. Chem. Soc. 126 (2004) 273–279, https://doi.org/10.1021/ja0380852.
[51] P. Kucheryavy, J. He, V.T. John, P. Maharjan, L. Spinu, G.Z. Goloverda, V.L. Kolesnichenko, Superparamagnetic Iron Oxide Nanoparticles with Variable Size and an Iron Oxidation State as Prospective Imaging Agents, (2012). https://doi.org/10.1021/la3037007.
[52] M.A. Ramos-Docampo, M. Testa-Anta, B. Rivas-Murias, V. Salgueiriño, Clusters of magnetite-maghemite nanocrystals with a chemically-tailored average diameter, J. Nanosci. Nanotechnol. 19 (2019) 4930–4937, https://doi.org/10.1166/jnn.2019.16788.
[53] R.G. Ruizmoreno, A.I. Martinez, R. Castro-Rodriguez, P. Bartolo, Synthesis and characterization of citrate coated magnetite nanoparticles, J. Supercond. Nov. Magn. 26 (2013) 709–712, https://doi.org/10.1007/s10948-012-1790-z.
[54] J. Biener, A. Wittstock, T.F. Baumann, J. Weissmüller, M. Bäumer, A.V. Hamza, Surface chemistry in nanoscale materials, Materials (basel). 2 (2009) 2404–2428, https://doi.org/10.3390/ma2042404.
[55] M. Mahmoudi, H.R. Kalhor, S. Laurent, I. Lynch, Protein fibrillation and nanoparticle interactions: opportunities and challenges, Nanoscale. 5 (2013) 2570–2588, https://doi.org/10.1039/c3nr33193h.
[56] Z. Ur Rahman, Y.L. Dong, C. Ren, Z.Y. Zhang, X. Chen, Protein adsorption on citrate modified magnetic nanoparticles, J. Nanosci. Nanotechnol. 12 (2012) 2598–2606, https://doi.org/10.1166/jnn.2012.5751.
[57] L. Shang, Y. Wang, J. Jiang, S. Dong, PH-dependent protein conformational changes in albumin: Gold nanoparticle bioconjugates: a spectroscopic study, Langmuir. 23 (2007) 2714–2721, https://doi.org/10.1021/la062064e.
[58] H. Suzuka, A. Mimura, Y. Inaoka, K. Murase, Magnetic nanoparticles in macrophages and cancer cells exhibit different signal behavior on magnetic particle imaging, J. Nanosci. Nanotechnol. 19 (2019) 6857–6865, https://doi.org/10.1166/jnn.2019.16619.
[59] B. Janic, A.S.M. Iskander, A.M. Rad, H. Soltanian-Zadeh, A.S. Arbab, Effects of ferumoxides - protamine sulfate labeling on immunomodulatory characteristics of macrophage-like THP-1 cells, PLoS One. 3 (2008) e2499.
[60] K. Müller, J.N. Skepper, M. Posfai, R. Trivedi, S. Howarth, C. Corot, E. Lancelot, P. W. Thompson, A.P. Brown, J.H. Gillard, Effect of ultrasmall superparamagnetic iron oxide nanoparticles (Ferumoxtran-10) on human monocyte-macrophages in vitro, Biomaterials. 28 (2007) 1629–1642, https://doi.org/10.1016/j.biomaterials.2006.12.003.
[61] P. Handa, S. Thomas, V. Morgan-Stevenson, B.D. Maliken, E. Gochanour, S. Boukhar, M.M. Yeh, K.V. Kowdley, Iron alters macrophage polarization status and leads to steatohepatitis and fibrogenesis, J. Leukoc. Biol. 105 (2019) 1015–1026, https://doi.org/10.1002/JLB.3A0318-108R.
[62] D. Reichel, M. Tripathi, J.M. Perez, Biological effects of nanoparticles on macrophage polarization in the tumor microenvironment, Nanotheranostics. 3 (2019) 66–88, https://doi.org/10.7150/ntno.30052.
[63] Y. Xia, Y. Li, X. Wu, Q. Zhang, S. Chen, X. Ma, M. Yu, Ironing out the details: how iron orchestrates macrophage polarization, Front. Immunol. 12 (2021), 669566, https://doi.org/10.3389/fimmu.2021.669566.
[64] A. Kroner, A.D. Greenhalgh, J.G. Zarruk, R. PassosdosSantos, M. Gaestel, S. David, TNF and increased intracellular iron alter macrophage polarization to a detrimental M1 phenotype in the injured spinal cord, Neuron. 83 (2014) 1098–1116, https://doi.org/10.1016/j.neuron.2014.07.027.
[65] Z.S. Gan, Q.Q. Wang, J.H. Li, X.L. Wang, Y.Z. Wang, H.H. Du, Iron reduces M1 macrophage polarization in RAW264.7 macrophages associated with inhibition of STAT1, Mediators Inflamm. (2017), https://doi.org/10.1155/2017/8570818.
[66] C. Gaetano, L. Massimo, M. Alberto, Control of iron homeostasis as a key component of macrophage polarization, Haematologica. 95 (2010) 1801–1803, https://doi.org/10.3324/haematol.2010.030239.
[67] J. Wosik, W. Chen, K. Qin, R.M. Ghobrial, J.Z. Kubiak, M. Kloc, Magnetic field changes macrophage phenotype, Biophys. J. 114 (2018) 2001–2013, https://doi.org/10.1016/j.bpj.2018.03.002.
[68] H. Ying, Y. Ruan, Z. Zeng, Y. Bai, J. Xu, S. Chen, Iron oxide nanoparticles size-dependently activate mouse primary macrophages via oxidative stress and endoplasmic reticulum stress, Int. Immunopharmacol. 105 (2022), 108533, https://doi.org/10.1016/j.intimp.2022.108533.
[69] S. Chen, S. Chen, Y. Zeng, L. Lin, C. Wu, Y. Ke, G. Liu, Size-dependent superparamagnetic iron oxide nanoparticles dictate interleukin-1β release from mouse bone marrow-derived macrophages, J. Appl. Toxicol. 38 (2018) 978–986, https://doi.org/10.1002/jat.3606.
[70] C. Polasky, T. Studt, A.-K. Steuer, K. Loyal, K. Lüdtke-Buzug, K.-L. Bruchhage, R. Pries, Impact of superparamagnetic iron oxide nanoparticles on THP-1 monocytes and monocyte-derived macrophages, Front. Mol. Biosci. 9 (2022), 811116, https://doi.org/10.3389/fmolb.2022.811116.